https://doi.org/10.5194/hess-2022-338
Preprint. Discussion started: 7 October 2022


Hydrology and Earth System Sciences
Discussions

# To what extent does river routing matter in hydrological modeling?

Nicolás Cortés-Salazar[1], Nicolás Vásquez[1], Naoki Mizukami[2], Pablo A. Mendoza[1,3], and Ximena Vargas[1]

[1]Department of Civil Engineering, Universidad de Chile, Santiago, Chile
[2]National Center for Atmospheric Research, Boulder, CO, USA
[3]Advanced Mining Technology Center, Universidad de Chile, Santiago, Chile

*Correspondence to*: Pablo A. Mendoza (pamendoz@uchile.cl)

**Abstract.**

Spatially-distributed hydrology and land surface models are typically applied in combination with river routing schemes that convert instantaneous runoff into streamflow. Nevertheless, the development of such schemes has been somehow disconnected from hydrologic model calibration research, although both seek to achieve more realistic streamflow simulations. In this paper, we seek to bridge this gap to understand the extent to which the configuration of routing schemes affects hydrologic model calibration results in water resources applications. To this end, we configure the Variable Infiltration Capacity (VIC) model, coupled with the mizuRoute routing model in the Cautín River basin (2770 km$^2$), Chile. We use the Latin Hypercube Sampling (LHS) method to generate 3500 different VIC model parameters sets, for which basin-averaged runoff estimates are obtained directly (no routing case), and subsequently compared against outputs from four routing schemes (Unit Hydrograph, Lagrangian Kinematic Wave, Muskingum-Cunge and Diffusive Wave) applied with five different routing time steps (1, 3, 6, 12 and 24 hours). The results show that incorporating routing schemes may alter streamflow simulations at sub-daily, daily and even monthly time scales. The maximum Kling-Gupta Efficiency (KGE) obtained for daily streamflow increases from 0.73 (no routing) to 0.82 (for the best scheme), and such improvements do not depend on the routing time step. Moreover, the optimal parameter sets may differ depending on the routing scheme configuration, affecting the baseflow contribution to total runoff. Including routing models decreases streamflow values in frequency curves and lowers the segment with high discharge values in the flow duration curve (compared to the case without routing). More generally, the results presented here highlight the potential impacts of river routing implementations on water resources applications that involve hydrologic models and, in particular, parameter calibration.

## 1. Introduction

Hydrology and land surface models are powerful tools to characterize the terrestrial water cycle, and provide valuable information for water resources planning under future climate scenarios (Vano et al., 2012; Mendoza et al., 2016; Melsen et al., 2018; Chegwidden et al., 2019). In applications at the catchment scale or beyond, these models are typically used in

https://doi.org/10.5194/hess-2022-338
Preprint. Discussion started: 7 October 2022


Hydrology and Earth System Sciences
Discussions

combination with river routing models that convert instantaneous runoff into realistic streamflow estimates at any locations in river networks (Oki and Sud, 1998; Olivera et al., 2000; Lucas-Picher et al., 2003). Hence, streamflow estimated by the river routing model is used for several water resources applications including flood risk assessments (Wobus et al., 2017), ecosystem health evaluations (Qiu et al., 2021), short-term streamflow forecasting (e.g., Tang et al., 2007; Emerton et al., 2016), and reservoir operations (Salas et al., 2018; Shaad, 2018).

Over the past three decades, many river routing models have been developed and coupled with hydrology and land surface models (Shaad, 2018). The river routing models vary in terms of modeling reservoir, irrigation and other human interventions on river water (e.g., Hanasaki et al., 2006), the spatial resolution and type of discretization of the river network – grid-based vs. vector-based (Lehner and Grill, 2013; Mizukami et al., 2016, 2021) – and, finally, the representation of flow physical processes in equations (hereafter, called routing scheme). The last category spans from a simple unit hydrograph method (Lohmann et al., 1996, 1998) to storage-based routing schemes such as Muskingum (David et al., 2011), simplifications of the Saint-Venant equations like kinematic wave (Decharme et al., 2010; Ye et al., 2013; Thober et al., 2019; Arora and Boer, 1999) or diffusive wave (Gong et al., 2009; Yamazaki et al., 2011), local inertia equations (Bates et al., 2010; Yamazaki et al., 2013) and full dynamic wave approaches (Paiva et al., 2011).

Given the wide range of routing methods available, it is crucial to understand benefits and limitations of each method for the specific model application (Shaad, 2018). Many studies have conducted intercomparison experiments with focus on routing schemes to evaluate their impacts on streamflow simulations. For example, Arora et al. (2001) compared a time-evolving (or variable velocity) algorithm that uses Manning's equation, against a simple storage-based routing scheme (without using momentum equation), operating at a very different horizontal resolution. Specifically, they concluded that the variable velocity scheme can produce higher values of peak discharge. Gong et al. (2009) demonstrated the benefits of diffusive wave routing over a linear reservoir routing method to get more realistic time delays in hydrograph waves in a basin located in southern China. David et al. (2011) introduced the Routing Application for Parallel Computation of Discharge (RAPID), based on the traditional Muskingum method (McCarthy, 1938), obtaining improvements in terms of Root Mean Squared Error (RMSE) and the Nash-Sutcliffe Efficiency (Nash and Sutcliffe, 1970) when compared to a lumped runoff scheme, which accumulate upstream instantaneous runoff without any delay. Ye et al. (2013) implemented a kinematic wave routing scheme in the Community Land Model (CLM) version 3.5, and obtained better results compared to the original grid-based River Transport Model (RTM), which uses the storage-based routing, in two basins in China.

More recently, Zhao et al. (2017) compared daily and monthly streamflow simulations produced with the CaMa-Flood (Yamazaki et al., 2011) model – fed with daily runoff from nine Global Hydrological Models (GHMs) – against those obtained with the same hydrological models and their native routing schemes (which have simpler physics). They concluded that the choice of routing scheme may have large effects on simulated streamflow and peak values. ElSaadani et al. (2018) compared streamflow simulations obtained from VIC runoff outputs using RAPID and the Hillslope Link Model (HLM; Mantilla, 2007), which is based on power laws that relate flow velocity, channel discharge and upstream area, at many stream gauges located in the Cedar River basin, Iowa. They noted that the choice of routing scheme has large effects on simulated hydrographs,

https://doi.org/10.5194/hess-2022-338
Preprint. Discussion started: 7 October 2022


Hydrology and Earth System Sciences
Discussions

obtaining more realistic peak times and magnitudes with the HLM model and decreasing differences in performance for larger catchments. Siqueira et al. (2018) compared a local inertia scheme against a non-hydrodynamic scheme or storage-based routing, showing that the former provided slight improvements in NSE and the Kling-Gupta efficiency (KGE; Gupta et al., 2009) over the Amazon and La Plata river basins, especially in flow timing. They highlighted that the calibration of hydrological parameters and including hydrodynamic routing are critical elements to achieve realistic streamflow simulations in South America.

Besides the complexity of the routing scheme used, the choice of routing time step may also impact streamflow calculations (Shaad, 2018). Qiu et al. (2021) characterized the effects of such decision on hydrological variables simulated with the SWAT model, which uses the variable storage coefficient routing scheme, computing flow velocity with the Manning equation. The authors used six time steps ranging from 1 minute to 1 day, and assessed their impacts on performance skills including NSE and bias, finding variations in streamflow simulations that were small compared to water storages and depth.

Although many past studies have shown that the choice of routing scheme affects streamflow simulations, efforts for improving their accuracy have been made by configuring hydrologic model and routing model independently: hydrologists still focus on parameter calibration to improve discharge simulations, neglecting the potential impacts of river routing configuration, especially routing scheme and time step (Newman et al., 2021; Beck et al., 2020), whereas routing model evaluation uses hydrologic model output, which contains varying degree of errors, making it difficult to evaluate routing models especially for basin or greater spatial domain (e.g., Mizukami et al., 2016; F. Zhao et al., 2017), and often use synthetic river discharge (David et al., 2011; Price, 2009).

In this paper, we seek to better understand the implications that the configuration of routing schemes may have when conducting hydrologic model calibration for water resources applications. To this end, we perform numerical experiments in the Cautín at Cajón River basin (Araucanía Region, Chile) using the Variable Infiltration Capacity (VIC) model (Liang et al., 1994) and the vector-based routing model mizuRoute (Mizukami et al., 2016). Specifically, we disentangle the impacts of hydrologic model parameters and different routing schemes (all implemented for five time steps) by combining a large sample of VIC simulations obtained from 3500 parameter sets, and routing simulations with four different routing methods implemented in mizuRoute. Our end goal is to unravel how the choice of routing method and routing time step affect (i) streamflow simulated at different temporal resolutions, (ii) performance metrics across the VIC parameter space, (iii) the selection of hydrologic model parameters given a target calibration metric, (iv) simulated water balance and runoff partitioning (i.e., baseflow ratio), and (v) hydrological signatures used for decision-making, including flood frequency curves and flow duration curves (FDCs). The results and conclusions drawn here reflect the impact that apparently innocuous modeling decisions may have for water resources management.

https://doi.org/10.5194/hess-2022-338
Preprint. Discussion started: 7 October 2022


Hydrology and Earth System Sciences
Discussions

## 2. Study domain and data

### 2.1 The Cautín River Basin

The study domain is the Cautín River basin (Figure 1), a sub-catchment of the Imperial River basin, located in the Araucanía Region, Chile. The basin elevation ranges between 125 and 3104 m a.s.l., the catchment area is 2770 km$^2$, and the dominant land cover types are crop-pasture rotation (44%) and native forest (40%). Additionally, the basin is prone to rainfall-driven flood events during winter and, therefore, has been subject of studies aimed to enhance predictive capabilities (e.g., Mendoza et al., 2012).

### 2.2 Hydrometeorological data

Daily precipitation, maximum and minimum temperature are obtained from the CR2MET v2.0 dataset (Boisier et al., 2018), which covers continental Chile with a horizontal resolution of 0.05° x 0.05° during the 1979-2020 period. In CR2MET, precipitation data was obtained with a statistical modeling framework that uses topographic descriptors and large-scale climatic variables (water vapor and moisture fluxes) from ERA5 (Hersbach, 2016) as predictors, and observed daily precipitation from gauge stations as predictand. For maximum and minimum daily temperature, additional variables from MODIS land surface products were added as predictors. Daily precipitation and temperature time series are disaggregated into hourly time steps using the sub-daily distribution provided by ERA5-Land (Muñoz-Sabater et al., 2021). Relative humidity, wind speed and shortwave radiation are derived for the same horizontal resolution grid by spatially interpolating ERA5-Land outputs. Longwave radiation was computed with the parameterization proposed by Iziomon et al. (2003), using CR2met air temperatures disaggregated to hourly time steps using the ERA5-Land hourly distribution.

Daily streamflow data is obtained from five stations (Figure 1) maintained by the Chilean Water Directorate (DGA, available at the CR$^2$ Climate Explorer https://www.cr2.cl/datos-de-caudales/). Similarly, hourly streamflow records for the CatC basin were obtained from the official DGA website ( https://dga.mop.gob.cl/servicioshidrometeorologicos).

## 3. Methods

### 3.1 Hydrological model

We use the VIC model (Liang et al., 1994) to simulate state variables and fluxes at a 0.05°x 0.05° horizontal resolution. VIC is a semi-distributed physically based hydrological model that solves energy and mass balance equations. Precipitation can be partitioned into snowfall or rainfall, and both can be stored in the canopy. The maximum amount of water intercepted by the canopy is estimated using the Leaf Area Index (LAI; Dickinson, 1984). The soil is represented by three layers controlling the infiltration (first soil layer) and baseflow (third soil layer). For infiltration fluxes, VIC uses the Xinanjiang formulation (Zhao, 1980), assuming that the infiltration capacity varies within an area (Wood et al., 1992). Excess runoff is generated in those areas where precipitation exceeds the amount of available soil moisture storage of the first soil layer. VIC assumes that drainage

https://doi.org/10.5194/hess-2022-338
Preprint. Discussion started: 7 October 2022


Hydrology and Earth System Sciences
Discussions

is driven by gravity, using the formulation proposed by Brooks & Corey (1964). In this regard, water enters the cell only from the atmosphere, i.e., VIC does not consider lateral fluxes among grid cells. Baseflow is generated in the third (deepest) soil layer using a formulation proposed by Franchini & Pacciani (1991). The snowpack is represented by two layers, where the top layer is used for energy balance computations (Andreadis and Lettenmaier, 2009). The reader is referred to Liang et al. (1994) for more details.

Horizontal heterogeneity is considered in each grid cell by incorporating different land cover types. Here, we use the IGBP classification for the year 2010 from the MCD12Q1 v006 land cover product (Sulla-Menashe and Friedl, 2018) to represent all land cover types spanning at least 2% of each grid cell area. Mean monthly LAI values for these land cover types are derived from the MOD15A2 product. Soil Bulk density is estimated using the mean value from the first 2 m depth of soil from the SoilGrids product (Poggio et al., 2021).

### 3.2 River network routing

mizuRoute first performs a hillslope routing using a gamma-distribution-based unit-hydrograph to delay instantaneous total runoff from the VIC model to a catchment outlet, and then route the delayed runoff for each river reach in the order defined by the river network topology. Full descriptions of hillslope routing and general routing procedures are provided in Mizukami et al. (2016). mizuRoute originally included two channel routing schemes: (1) kinematic wave tracking (KWT) routing, and (2) impulse response function (IRF) routing, which is similar to the Lohmann et al. (1996) model except that mizuRoute uses a reach-to-reach routing approach instead of the source-to-sink approach. Details of both routing schemes are also provided in Mizukami et al. (2016). Here, we implement in mizuRoute two additional routing schemes commonly used for many water resources applications: Diffusive Wave routing (DW, Appendix A) and Muskingum Cunge (MC, Appendix B). All the channel routing schemes except IRF (which uses prescribed wave celerity and diffusivity) share two parameters: Manning's n roughness coefficient and channel width (assuming rectangular channel).

In this work, we derive an "a priori" spatial distribution of Manning's n roughness coefficient for the entire river network through a two-step procedure: (i) we develop a relationship between the roughness $n_0$ and channel slope using data from 50 Chilean rivers (Niño, 2002), and (ii) we use in situ observations conducted by Mendoza et al. (2012) to correct $n_0$ based on a statistical relationship with n values estimated at 46 locations in the Cautín River basin. Additionally, we use the relationship between channel width and drainage area developed by Mendoza et al. (2012) to obtain spatially distributed river width values.

### 3.3 Sampling of VIC parameters

To examine the impacts of different routing schemes on streamflow performance metrics across the VIC parameter space, we use 3500 parameters sets obtained with the Latin Hypercube Sampling (LHS) method. Here, we consider the parameters identified by Sepúlveda et al. (2022) as the most sensitive (Table 2). For each parameter set, we run VIC at hourly time steps for the period April/2006 - March/2012, and the results are temporally aggregated to 3-hour, 6-hour, 12-hour and 24-hour

https://doi.org/10.5194/hess-2022-338
Preprint. Discussion started: 7 October 2022


Hydrology and Earth System Sciences
Discussions

resolutions to subsequently run mizuRoute for the same time steps using the Impulse Response Function (IRF), Kinematic Wave (KW), Muskingum-Cunge (MC) and Diffusive Wave (DW). For completeness, we also compute streamflow using spatially-averaged total runoff within each basin (hereafter referred to as instantaneous runoff, Inst), which is a common approach used in hydrological modeling applications (Mendoza et al., 2016; Beck et al., 2020). As a result, we obtain streamflow times series at each river reach (Figure 1c) for five routing schemes (including no routing as the baseline) and five temporal resolutions (1 h, 3 h, 6 h, 12 h and 24 h).

### 3.4 Objective functions

We evaluate the performance of streamflow simulations from VIC-mizuRoute using two metrics: (i) the Nash-Sutcliffe efficiency (NSE; Nash & Sutcliffe, 1970) and (ii) the Kling Gupta efficiency (KGE; Gupta et al., 2009; Kling et al., 2012). The NSE metric is computed using observed (o) and simulated (s) streamflow ($Q$):

$$NSE(Q) = 1 - \frac{\sum_{t=1}^{n}(Q_o^t - Q_s^t)^2}{\sum_{t=1}^{n}(Q_o^t - \bar{Q}_o)^2} \quad (1)$$

Where $Q_o^t$ is the observed streamflow for time step $t$, $Q_s^t$ is the simulated streamflow for time step $t$ and $\bar{Q}_o$ is the mean observed streamflow over the $n$ time steps considered. Similarly, the KGE quantifies performance in terms of variability, volume and timing:

$$KGE(Q) = 1 - \sqrt{(1-\alpha)^2 + (1-\beta)^2 + (1-r)^2} \qquad \alpha = \frac{\sigma_s}{\sigma_o} \qquad \beta = \frac{\mu_s}{\mu_o} \quad (2)$$

where $\sigma$ is the standard deviation for simulated and observed values, $\mu$ is the mean streamflow over the $n$ times steps, and $r$ is the Pearson correlation coefficient between simulated and observed streamflow. Both metrics (NSE and KGE) range between $-\infty$ and 1, where 1 represents a perfect simulation. The NSE is also computed for the logarithms of the streamflow (NSE-log) to test the model's capability to simulate low flows (Krause et al., 2005).

The three objective functions are calculated for the period April/2008 – March/2012, using all the combinations of VIC parameter sets (3500), routing schemes (including the case without routing) and routing time steps (1h, 3 h, 6 h, 12 h and 24 h). Additionally, for each routing time step, the calibration metrics are computed for different aggregated time step when possible. For example, to estimate metrics at an hourly time step, routing can only be run at a 1-hour time step. Metrics computed at 3-hourly time steps use temporally averaged streamflow from a 1-hour and 3-hour mizuRoute simulations. Metrics computed at 6-hourly time steps can be computed from temporally averaged 1-hour, 3-hour and 6-hours mizuRoute simulations, and so on. The observed streamflow for a given time step is estimated from hourly streamflow records.

### 3.5 Analysis framework

Figure 2 summarizes the methodology used here. To evaluate the impact of river routing configurations on calibration results, we select (from the large sample described in section 3.3) the VIC parameter set that maximizes, for a specific combination of routing scheme and routing time step, each objective function at each stream gauge station (Figure 1, Table 1). Hence, for each

https://doi.org/10.5194/hess-2022-338
Preprint. Discussion started: 7 October 2022


Hydrology and Earth System Sciences
Discussions

calibration metric we obtain 5 (number of routing scheme options) x 5 (number of routing time steps) best parameter sets that are used for subsequent analyses. For the KWT scheme, we select two additional VIC parameter sets for the cases of spatially constant $n_0$ values of 0.01 (default option) and 0.03 (i.e., the spatially constant value used by Yamazaki et al., 2011).

First, we illustrate the effect of routing modeling decisions – specifically, routing time step, routing scheme and spatial distribution of the Manning's roughness coefficient – on simulated daily hydrographs at Cautín at Cajón. Additionally, we examine the impact of excluding the river routing process on simulated streamflow at annual, monthly, daily and sub-daily time steps.

We also analyze the impact of routing configurations on model performance and selected VIC parameter values. First, we explore the overall impact of routing scheme and routing time step on performance metrics (section 3.4) computed with different temporal resolutions across the VIC parameter space (Figure 2c). Then, we examine the sensitivity of the best objective function value (achievable from the LHS results) in each sub-catchment to river routing configuration, and its effects on simulated annual water balance (specifically, the mean annual runoff ratio) and baseflow contribution to total runoff (Figure 2d.1); and VIC parameter values (Figure 2d.2).

Because high flows are relevant for engineering applications, in particular, infrastructure design, we also analyse the implications of routing configurations for the calculation of flood frequency curves (Figure 2e.1). To this end, we run VIC at hourly time steps from April/1981 to March/2020 using the parameters associated to the highest KGE and NSE values for each routing configuration. Then, hourly VIC total runoff is aggregated and routed at different time steps (i.e., 3 h, 6 h, 12 h and 24 h), and annual maximum daily flows are obtained for the period April/1985 – March/2020 (i.e., the period April/1981 – March/1985 is dropped). Hence, for each routing time step we obtain five annual time series with n = 35 values (obtained from the baseline and the four routing schemes) that are used to compute maximum daily flows at return periods of 20, 50, 100, 200, 500 and 1000 years. We use the Log-Normal parametric distribution – which provides the best results for the Kolmogorov–Smirnov test – for the observed time series of maximum daily flows. Finally, we characterize the impacts of routing configurations on flow duration curves, which are widely used in water resources applications (Figure 2e.2).

## 4. Results

### 4.1 Illustration of routing effects

Figure 3 illustrates the sensitivity of daily streamflow simulations to different routing modeling decisions, including the effects of routing time step on IRF scheme (Figure 3a), the impact of routing schemes for daily routing time step (Figure 3b), and the impact of the Manning's roughness coefficient on KWT results (Figure 3c). In each panel, simulations are obtained for the 2008 Fall/Winter seasons (when most of the total precipitation occurs) using the parameter set (obtained from LHS) that maximizes the KGE for each combination of routing scheme, routing time step and Manning's coefficient distribution. To enable the comparison among different options, sub-daily routing simulations are aggregated to a 24-hour time step. One can note that the routing time step and the routing scheme have a larger effect on peak discharge values. Additionally, increasing

https://doi.org/10.5194/hess-2022-338
Preprint. Discussion started: 7 October 2022


Hydrology and Earth System Sciences
Discussions

routing time steps for IRF accelerates the timing of peak discharge, though decreasing its value. The choice of routing scheme affects the shape of storm hydrographs, especially high flows. Finally, a uniform value of n = 0.03 and the spatially distributed configuration of the Manning's roughness coefficient yield a delay in peak flow simulations.

Figure 4 compares streamflow obtained from mizuRoute (y-axis) against instantaneous runoff (x-axis, no routing) for several temporal resolutions and different routing schemes. In this case, the parameter set used to run the VIC model is the one that maximizes the KGE among the 3500 parameter sets from the LHS. The results for hourly time steps show that the lack of routing yields much larger values (> 1700 $m^3/s$ in some cases) compared to routed streamflow. These differences are gradually reduced when the routing time step increases to $\Delta t$ = 3 h and 6 h, although differences can be larger than 1200 $m^3/s$. The impact of excluding routing reduces as the time step increases, although it can be important even for $\Delta t$ = 24 h time step. At monthly time steps, the differences between routed and instantaneous runoff reduce drastically, becoming negligible at the annual resolution. Further, such differences are very similar for other time steps across routing schemes, although slight differences in $r^2$ suggest that IRF and KWT affect more VIC outputs.

### 4.2 Effects on performance metrics

The KGE, NSE and NSE-log values at Cautín at Cajón obtained from the 3500 VIC parameters sets, routing schemes and routing time steps are displayed in Figure 5. To compare performance measures from different configurations, simulations were aggregated to the metric time resolution (columns, see details in section 3.5). Overall, the results show a clear difference between including routing and no routing. Indeed, the maximum KGE is close to 0.7 for instantaneous runoff, increasing to ~0.8 when routing is included, regardless of the time step used to compute the metric or run the routing model. Similar improvements are observed for NSE, with increments that can be larger than 0.3 NSE units, depending on the time step to compute the streamflow metric (e.g., 1 h). Finally, smaller differences are obtained for NSE-log among routing configurations, mainly due to the minor influence of high flow values on the metric.

Figure 6 compares the best KGE, NSE and NSE-log values (computed from daily flows) achievable from the large sample of VIC parameters in each basin (represented by the basin area in the x-axis), given a specific combination of routing scheme and routing time step. For completeness, the KGE components ($\alpha$, $\beta$ and $r$) are also displayed. For all objective functions and catchments, the maximum (highest) values increase when the routing process is included, regardless of the river routing configuration. Very similar maximum KGE values are obtained with the four schemes implemented in mizuRoute, and the differences among these schemes are generally lower than 0.05 KGE units for all time steps and basins. The differences in KGE due to the incorporation of routing are larger than differences among the four routing schemes; in particular, routing yields increments >0.1 in KGE for Cautin at Rariruca (1305 $km^2$), which are mainly explained by variations in the ratio of mean values ($\beta$) and temporal correlation ($r$). Indeed, the low $r$ values of simulated instantaneous runoff can be largely improved by changing the timing of high peak flows through the addition of routing processes. Figure 6 also shows considerable improvements in NSE across all catchments when routing is applied. Notably, differences between routing and no routing options are also obtained for NSE-log.

https://doi.org/10.5194/hess-2022-338
Preprint. Discussion started: 7 October 2022


Hydrology and Earth System Sciences
Discussions

Finally, the results in Figure 6 suggest that implementing routing schemes yields benefits in the timing of simulated streamflow (compared to the baseline case) as contributing area increases. Nevertheless, there is not a clear relationship between the latter variable and performance metrics.

### 4.3 Impact on simulated fluxes and VIC parameters

Figure 7 illustrates, for each routing time step (columns) and calibration objective function (all computed with daily discharge and displayed in different rows), the impacts of the choice of routing scheme on the partitioning of the mean annual runoff ratio (x-axis) and the ratio between mean annual baseflow and mean annual total runoff (y-axis) for the period April/2008-March/2012. To account for equifinality effects, we also include VIC parameter sets with calibration metric values within the 0.1% best simulations. For KGE and NSE, excluding routing (Inst, represented by squares) forces VIC to compensate the absence of this process by delaying the runoff response with a larger contribution of baseflow to total runoff, compared to any routing scheme. When the VIC model parameters are selected based on the NSE-log metric, the differences provided by routing configuration options are smaller compared to KGE and NSE.

Figure 7 also shows that NSE is the only metric for which slight differences in Q/P arise between Inst and routing schemes. In such case, higher annual runoff ratios (and hence a lower evaporative ratio) are obtained when routing processes are ignored, regardless of the routing time step selected. Additionally, we do not find any clear relationship between baseflow contribution (bf/Q) or precipitation partitioning (Q/P) with the choice of routing scheme.

To examine the effect of river routing on the selection of VIC parameters, we choose, for each combination of routing time step and routing scheme, the best (highest) value for NSE, KGE and NSE-log (computed with daily flows) among the 3500 parameter sets from LHS (Figure 8). The parameters values are normalized by the difference between the maximum and minimum values obtained from LHS to facilitate comparisons. Hence, a normalized value of zero indicates the lower boundary of the parameter, while a value of 1 indicates the upper limit. The results indicate that the same best parameter set is obtained for NSE-log regardless of the selected routing scheme or the routing time step. For NSE, including routing yields a different VIC parameter set, which is the same for all routing schemes implemented in mizuRoute. Conversely, for KGE the choice of routing scheme may affect the selected VIC parameter set. Indeed, selecting IRF results in a different parameter set for routing time steps larger than 3-hours. It should be noted that, for both NSE and (especially) KGE, excluding routing (Inst) produces higher values for the soil parameters $W_s$ (fraction of maximum soil moisture where non-linear baseflow occurs) and $K_{sat}$ (saturated hydraulic conductivity), regardless of the routing time step.

The results displayed in Figure 8 also show that different metric values may be achieved with the same VIC parameters when modifying only the routing scheme. For example, if NSE is the calibration criteria and $\Delta t = 3$ h, the NSE values obtained using IRF and DW (with the same VIC parameter values) are 0.700 and 0.774, respectively. Similar variations are obtained for KGE, highlighting the importance of the choice of routing scheme when characterizing streamflow performance.

https://doi.org/10.5194/hess-2022-338
Preprint. Discussion started: 7 October 2022


Hydrology and Earth System Sciences
Discussions

### 4.4 Implications for flood frequency and flow duration curves

Figure 9 shows the flood frequency curves obtained from annual time series of maximum daily flows (see details in Section 3.5), using KGE and NSE at daily time steps as objective functions. Note that the curve for daily instantaneous runoff is the same for each metric (i.e., the same across rows). The panels in the two bottom rows zoom into maximum annual daily flows for a return period T = 100 years. The results show that the choice of routing time step impacts frequency analyses. For example, for a routing time step of 1-hour, the spread provided by different routing schemes is small across return periods. However, the dispersion among routing schemes increases with larger Δt. For T = 100 years, the differences among routing schemes for routing time step Δt = 1 h are smaller than 100 $m^3/s$, while for Δt = 12 h or Δt = 24 h the differences can be as large as 200 $m^3/s$.

Figure 10 shows daily FDCs obtained with different routing schemes, different routing time steps (columns) and VIC parameters that maximize NSE or KGE (rows). The bottom panels zoom into discharge values with low exceedance probabilities (0-1%). When the objective function is KGE, differences arising from the choice of routing scheme are generally small for medium and low flows, though such differences increase for low exceedance probabilities (0-0.01). In such cases, the impacts of including river routing are noticeable, and for $\Delta t \geq 6$ h IRF results depart from the remaining routing methods. For NSE, including the routing process impacts the medium and low flow segments of the FDC (as opposed to KGE). Further, inter-method differences for high flow values can be larger compared to the differences between instantaneous vs. routed runoff (see results for $\Delta t \geq 6$ h).

## 5. Discussion

### 5.1 Implications for hydrological modeling

In this paper, we use the LHS approach to evaluate the impact of routing on streamflow performance metrics across the parameter space. Our results suggest that, regardless of the routing scheme, including this process improves the overall streamflow performance (Figures 5 and 6). Nevertheless, such conclusion may depend on the hydrological regime of the catchment and the distributed spatial configuration of the river routing implementation. The Cautín River basin has a rainfall-dominated runoff regime, with high flow peaks associated to heavy rainfall events during the winter season, and a slight influence of snowmelt during the spring season. Indeed, the catchment response time and peak discharge depend on the runoff routing process in the river network; hence, its explicit inclusion in hydrological modelling may yield better results, especially for performance metrics influenced by high flows (Clark et al., 2021). However, the differences between routed and non-routed runoff are less evident for NSE-log.

The effects of including river routing are also reflected in the partitioning of total runoff. Indeed, the results presented here show that calibration compensates for the lack of routing by modifying other fluxes and state variables (Khatami et al., 2019) to increase streamflow-oriented performance metrics. In our case, the contribution of baseflow to total runoff increases by

https://doi.org/10.5194/hess-2022-338
Preprint. Discussion started: 7 October 2022


Hydrology and Earth System Sciences
Discussions

>20% when river routing is not included, which is achieved by modifying soil parameters –especially $W_s$, previously identified as one of the most sensitive for baseflow processes (Sepúlveda et al., 2022) – to delay the streamflow response. Conversely, we did not find considerable changes in the partitioning of precipitation between evapotranspiration and runoff in the absence of river routing.

Most of our analyses show similar results with all routing schemes except for IRF, which has different implications for high flows (Figures 9 and 10). Even more, Figure 8 shows that the optimal parameter set identified for each routing scheme is the same for KWT, MC and DW if we use a high flow-oriented calibration metric like KGE and NSE, indicating that these results are not consequence of compensation from calibration exercise. The smaller difference among these three methods may be explained by the use of the same parameter set, Manning coefficients and channel width, while IRF uses prescribed wave celerity and diffusivity as model parameters (recall that we did not calibrate any routing parameters). Also, because the slope of river reaches in the Cautín river basin ranges from 0.0004 to 0.274 m/m, selecting kinematic wave-based (i.e., KWT) or diffusive wave routing schemes may have less impacts. More benefits of using diffusive wave routing are typically expected for flatter river systems (slope < 0.001 m/m; e.g., Kazezyılmaz-Alhan et al., 2007), where flood wave diffusion processes dominate.

Although the routing time step does not affect performance metrics considerably in our experimental setup, it can affect the choice of VIC parameter values (e.g., see results for KGE), which is in line with previous hydrologic modeling research. For example, Kavetski et al. (2011) found that temporal data resolution may alter parameter values in conceptual hydrological models. More recently, Melsen et al. (2016) found that the parameter values may greatly vary if calibration metrics are computed at hourly, daily or monthly time steps.

### 5.2 Limitations and future work

Here, we only focused on the choice of routing scheme and routing time step, though there are many other decisions that could be explored in the implementation of river routing models. For example, we did not examine the effects of surface storage elements like reservoirs, wetlands, and flood plains on river flow dynamics. Additionally, we did not calibrate routing parameters, which means that differences in performance obtained with different routing schemes may be attributed to the parameter values adopted by default. However, past studies have found that the parameter values of river routing schemes are relevant to achieve good results (Boyle et al., 2001; Butts et al., 2004). Therefore, future studies should characterize, for a given combination of hydrology model and routing scheme, parameter sensitivities before the calibration process (e.g., Huang and Liang, 2006; Mai et al., 2020). Recently, Sheikholeslami et al. (2021) conducted a variance-based sensitivity analysis to the VIC model coupled with the IRF routing scheme (implemented with mizuRoute) in a nivo-glacial basin, finding that two routing parameters are highly relevant to reproduce the observed peak time and flashiness in the hydrograph. Such analyses could be repeated with the remaining routing schemes, adopting spatial regularization strategies for hydraulic parameters if needed (e.g., Mendoza et al., 2012).

https://doi.org/10.5194/hess-2022-338
Preprint. Discussion started: 7 October 2022


Hydrology and Earth System Sciences
Discussions

In this study, we did not use the dynamic wave approximation, which might yield improvements compared to the routing schemes tested here, especially very large flood events at downstream of the bases or flatter part of basins. Indeed, Paiva et al. (2013b) validated a full hydrodynamic model in stream gauges within the Amazon River basin, obtaining that discharge and water levels were simulated accurately, outperforming the MC approach. The same model was evaluated against satellite observations, showing good performance in terms of water levels and inundation extents (Paiva et al., 2013a). Hence, future assessments of routing schemes may include more detailed comparisons against remotely sensed data, adding catchments with different hydrological regimes (e.g., snowmelt-driven, mixed regimes) and physiographic characteristics (e.g., contributing area, average slope, land cover types). Further, it would be interesting to examine the interplay between structural uncertainty and parametric uncertainty in river routing models, a topic that has been widely explored in the hydrologic modeling literature (e.g., Ajami et al., 2007; Günther et al., 2019; Newman et al., 2021).

One advantage over previous studies was the availability of field measurements to estimate the spatial variability of the Manning's roughness coefficient (*n*) across the Cautín River basin. Due to data restrictions, many past studies used spatially constant values of *n* (Lucas-Picher et al., 2003; Yamazaki et al., 2011; Arora and Boer, 1999; Siqueira et al., 2018), or have adopted indirect approaches. For instance, Decharme et al. (2010) estimated *n* as a linear function of the river width W; Miguez-Macho & Fan (2012) used satellite land cover to assign the Manning's roughness coefficient and Verzano et al. (2012) estimated *n* variability in space based on topography, the location of urban population, and river sinuosity. More detailed assessments than the one presented here would be useful to determine the most effective and efficient approach to estimate *n* fields.

## 6. Conclusions

Despite the general consensus in the hydrology and Earth system modeling communities about the relevance of river routing schemes for realistic streamflow simulations, there is little knowledge on the extent to which this process is relevant. Additionally, hydrologic model calibration research has been done neglecting the impacts of river routing model configurations, and routing model development has been conducted ignoring the effects of hydrologic model parameters. In this paper, we try to fill these gaps by performing modeling experiments at the Cautín River basin (Chile), coupling the VIC model simulations obtained from an ensemble of 3500 parameter sets, with four different routing schemes implemented in mizuRoute at various time steps.

Our main conclusions are as follows:

1. Runoff routing alters streamflow simulations considerably at sub-daily and daily time steps, with slight (negligible) impacts at the monthly (annual) time step.
2. Including a river routing model may provide better hydrologic model calibration results compared to the case without routing.
3. The timing of streamflow simulations may improve for larger contributing areas if runoff routing is performed.

https://doi.org/10.5194/hess-2022-338
Preprint. Discussion started: 7 October 2022


Hydrology and Earth System Sciences
Discussions

4. Including routing processes may yield different calibrated parameter sets for daily metrics KGE($Q_{24h}$) and NSE($Q_{24h}$) compared to the case without routing, and different routing methods may yield different hydrologic parameter sets, with notable impacts on the baseflow contribution to total runoff.
5. Including routing models decreases annual maximum daily flows values in frequency curves and the segment with high flow volumes in the FDC (compared to the case without routing). Additionally, differences among routing schemes in these curves increases with larger routing time steps.
6. When the calibration metric is NSE($Q_{24h}$), including routing models may affect the probabilistic distribution of medium and low daily flows.

**Appendix A. Diffusive wave routing**

The flood wave propagation through a river channel is described with the 1-dimensional Saint-Venant equations:

$$\frac{\partial Q}{\partial x}+\frac{\partial A}{\partial t}=0 \quad \text{(Eq. A1)}$$

$$\frac{\partial Q}{\partial t}+\frac{\partial}{\partial x}\left(\frac{Q^2}{A}\right)+gA\frac{\partial Z}{\partial x}-gA(S_o-S_f)=0 \quad \text{(Eq. A2)}$$

where $Q$ is discharge [$L^3T^{-1}$] at time step $t$ [T] and location $x$ [L] in a river reach, $A$ is cross-sectional flow area [$L^2$], $Z$ is flow depth [L], $S_0$ is channel slope [-], $S_f$ is friction slope [-], and $g$ is gravitational constant [$LT^{-2}$]. The continuity equation (Eq .A1) assumes that no lateral flow is added to a channel segment. A friction slope is expressed using channel conveyance $K_c$:

$$S_f=\frac{Q|Q|}{K_c} \quad \text{(Eq. A3)}$$

In large domain river routing, one-dimensional full Saint-Venant equations, or fully dynamic wave equations, are typically simplified by neglecting some force terms in the momentum equation (Eq. A2). The kinematic wave approximation is obtained by neglecting acceleration and pressure gradient terms, assuming that river bed slope and energy slope are equal. This assumption is the basis of the kinematic wave tracking algorithm (Mizukami et al., 2016). If a rectangular channel with a channel width $w$ is used, the diffusive wave equation can be obtained by neglecting acceleration terms (1st and 2nd terms in Eq. A2) and combining Eqs. A1 and A2 (Sturm, 2021):

$$\frac{\partial Q}{\partial t}=D\frac{\partial^2 Q}{\partial x^2}-C\frac{\partial Q}{\partial x} \quad \text{(Eq. A4)}$$

Where:

$$C=\frac{1}{K_c}\frac{dK_c}{dA}=\frac{dQ}{dA}$$

$$D=\frac{K_c^2}{2qw}=\frac{Q}{2wS_o}$$

where $K_c$ is conveyance, and parameters $C$ and $D$ are wave celerity [$LT^{-1}$] and diffusivity [$L^2T^{-1}$], respectively.

https://doi.org/10.5194/hess-2022-338
Preprint. Discussion started: 7 October 2022


Hydrology and Earth System Sciences
Discussions

To solve the diffusive wave equation for discharge *Q*, Eq. A4 is discretized using weighted averaged finite difference approximations across two time steps in space (i.e., 2nd-order central difference in the 1st term in A4, and 1st order central difference for 2nd term in A4). The resulting discretized diffusive wave equation is:

$$(\alpha C_a - 2\beta C_d)\cdot Q_{j+1}^{t+1} + (2 + 4\beta C_d)\cdot Q_j^{t+1} - (\alpha C_a + 2\beta C_d)\cdot Q_{j-1}^{t+1}$$
$$= -[(1-\alpha)C_d - 2(1-\beta)C_d]\cdot Q_{j+1}^{t} + [2 - 4(1-\beta)C_d]\cdot Q_j^{t} + [(1-\alpha)C_a + 2(1-\beta)C_d]\cdot Q_{j-1}^{t}$$

$$C_a = \frac{C\cdot\Delta t}{\Delta x} \qquad C_d = \frac{D\cdot\Delta t}{(\Delta x)^2} \qquad \text{(Eq. A5)}$$

Where α is weight factor for the 1st order space difference approximation of the second term in Eq. A4, and β is a weight factor for the 2nd order space difference approximation of the first term in Eq. A4. If both weights are set to 1, the finite difference becomes a fully implicit scheme, while setting both weights to zero results in a fully explicit scheme.

If internal nodes are defined within each reach (here we used 5), Eq. A5 becomes a system of linear equations that can be expressed in tridiagonal matrix form and solved with the Thomas' algorithm. In this paper, we use a fully implicit finite difference approximation (i.e., α = β =1). The solution of the implicit method requires downstream and upstream boundary conditions, being the latter inflow from upstream reaches. We use the Neumann boundary condition, which specifies the gradient of discharge between the current and downstream reaches. Note that in diffusive wave routing, celerity (*C*) and diffusivity (*D*) are updated at every time step based on the discharges (*Q*) and flow area (*A*), as opposed to IRF routing in which celerity and diffusivity are provided as model parameters.

**Appendix B. Muskingum-Cunge**

In the Muskingum-Cunge (MC) routing approach, the desired streamflow value is computed as the weighted ($C_1$, $C_2$, and $C_3$) average of known discharge values at upstream and downstream positions, at current and previous time steps:

$$Q_{j+1}^{t+1} = C_1\cdot Q_j^t + C_2\cdot Q_{j+1}^t + C_3\cdot Q_j^{t+1} \qquad \text{(Eq. A6)}$$

$$C_1 = \frac{2KX + \Delta t}{2K(1-X) + \Delta x} \qquad C_2 = \frac{2K(1-X) - \Delta t}{2K(1-X) + \Delta x} \qquad C_3 = \frac{-2KX + \Delta t}{2K(1-X) + \Delta x}$$

The parameters *K* and *X* are defined as;

$$K = \frac{\Delta x}{C} \qquad X = 0.5 - \frac{Q}{2S_o C\Delta x}$$

Here, both parameters are computed with discharge *Q* updated at every time step based on the average of inflow at the current time step and inflow and outflow at the previous time step. Note that celerity is also a function of discharge. Since Muskingum-Cunge is an explicit method, the routing time step can affect the numerical stability of the solution. To stabilize the solution, sub-routing time step is determined so that Courant condition (C*dT/dx where C is wave celerity [L/T], dT is routing time step [T] and dx is channel length [L]) is less than unity.

https://doi.org/10.5194/hess-2022-338
Preprint. Discussion started: 7 October 2022


Hydrology and Earth System Sciences
Discussions

## Code availability

The codes used in this study are available from the corresponding author upon reasonable request.

## Author contributions

All the authors were involved in the conceptualization of this study. NC, NV, NM and PM designed the methodology and analysis framework and drafted the paper. NV configured the VIC model. NM developed all the routing schemes in mizuRoute. NC configured mizuRoute, conducted simulations, analysed the results and created the figures. XV provided insights into the analysis results. All the authors discussed the results and contributed to writing, reviewing and editing the manuscript.

## Competing interests

The authors declare that they have no conflict of interest.

## Acknowledgments

Pablo A. Mendoza received support from Fondecyt Project 11200142 and CONICYT/PIA Project AFB180004.

## References

Ajami, N. K., Duan, Q., and Sorooshian, S.: An integrated hydrologic Bayesian multimodel combination framework: Confronting input, parameter, and model structural uncertainty in hydrologic prediction, Water Resour. Res., 43, W01403, https://doi.org/10.1029/2005WR004745, 2007.

Andreadis, K. ~M. and Lettenmaier, D. ~P.: Predicting snowpack stratigraphy in forested environments, in: EGU General Assembly Conference Abstracts, 11901, 2009.

Arora, V., Seglenieks, F., Kouwen, N., and Soulis, E.: Scaling aspects of river flow routing, Hydrol. Process., 15, 461–477, https://doi.org/10.1002/hyp.161, 2001.

Arora, V. K. and Boer, G. J.: A variable velocity flow routing algorithm for GCMs, J. Geophys. Res. Atmos., 104, 30965–30979, https://doi.org/10.1029/1999JD900905, 1999.

Bates, P. D., Horritt, M. S., and Fewtrell, T. J.: A simple inertial formulation of the shallow water equations for efficient two-dimensional flood inundation modelling, J. Hydrol., 387, 33–45, https://doi.org/10.1016/j.jhydrol.2010.03.027, 2010.

Beck, H. E., Pan, M., Lin, P., Seibert, J., van Dijk, A. I. J. M., and Wood, E. F.: Global Fully Distributed Parameter Regionalization Based on Observed Streamflow From 4,229 Headwater Catchments, J. Geophys. Res. Atmos., 125,


https://doi.org/10.1029/2019JD031485, 2020.

Boisier, J. P., Alvarez-Garretón, C., Cepeda, J., Osses, A., Vásquez, N., and Rondanelli, R.: CR2MET: A high-resolution precipitation and temperature dataset for hydroclimatic research in Chile, in: EGU General Assembly Conference Abstracts, 19739, 2018.

Boyle, D. P., Gupta, H. V., Sorooshian, S., Koren, V., Zhang, Z., and Smith, M.: Toward improved streamflow forecasts: Value of semidistributed modeling, Water Resour. Res., 37, 2749–2759, https://doi.org/10.1029/2000WR000207, 2001.

Brooks, R. H. and Corey, A. T.: Hydraulic properties of porous media. Hydrology Paper 1964, № 3, Civ. Eng. Dep., Color. State Univ., Fort Collins, Color. 27pp, 1964.

Butts, M. B., Payne, J. T., Kristensen, M., and Madsen, H.: An evaluation of the impact of model structure on hydrological modelling uncertainty for streamflow simulation, J. Hydrol., 298, 242–266, https://doi.org/10.1016/j.jhydrol.2004.03.042, 2004.

Chegwidden, O. S. S., Nijssen, B., Rupp, D. E. E., Arnold, J. R. R., Clark, M. P. P., Hamman, J. J. J., Kao, S. C. S. C., Mao, Y., Mizukami, N., Mote, P. W., Pan, M., Pytlak, E., and Xiao, M.: How do modeling decisions affect the spread among hydrologic climate change projections? Exploring a large ensemble of simulations across a diversity of hydroclimates, Earth's Futur., 7, 623–637, https://doi.org/10.1029/2018EF001047, 2019.

Clark, M. P., Vogel, R. M., Lamontagne, J. R., Mizukami, N., Knoben, W. J. M., Tang, G., Gharari, S., Freer, J. E., Whitfield, P. H., Shook, K. R., and Papalexiou, S. M.: The Abuse of Popular Performance Metrics in Hydrologic Modeling, Water Resour. Res., 57, 1–16, https://doi.org/10.1029/2020WR029001, 2021.

David, C. H., Maidment, D. R., Niu, G. Y., Yang, Z. L., Habets, F., and Eijkhout, V.: River network routing on the NHDPlus dataset, J. Hydrometeorol., 12, 913–934, https://doi.org/10.1175/2011JHM1345.1, 2011.

Decharme, B., Alkama, R., Douville, H., Becker, M., and Cazenave, A.: Global Evaluation of the ISBA-TRIP Continental Hydrological System. Part II: Uncertainties in River Routing Simulation Related to Flow Velocity and Groundwater Storage, J. Hydrometeorol., 11, 601–617, https://doi.org/10.1175/2010JHM1212.1, 2010.

Dickinson, R. E.: Modeling Evapotranspiration for Three-Dimensional Global Climate Models, in: Climate Processes and Climate Sensitivity, American Geophysical Union (AGU), 58–72, https://doi.org/https://doi.org/10.1029/GM029p0058, 1984.

ElSaadani, M., Krajewski, W. F. F., Goska, R., and Smith, M. B. B.: An Investigation of Errors in Distributed Models' Stream Discharge Prediction Due to Channel Routing, J. Am. Water Resour. Assoc., 54, 742–751, https://doi.org/10.1111/1752-1688.12627, 2018.

Emerton, R. E., Stephens, E. M., Pappenberger, F., Pagano, T. C., Weerts, A. H., Wood, A. W., Salamon, P., Brown, J. D., Hjerdt, N., Donnelly, C., Baugh, C. A., and Cloke, H. L.: Continental and global scale flood forecasting systems, Wiley Interdiscip. Rev. Water, 3, n/a-n/a, https://doi.org/10.1002/wat2.1137, 2016.

Franchini, M. and Pacciani, M.: Comparative analysis of several conceptual rainfall-runoff models, J. Hydrol., 122, 161–219, https://doi.org/https://doi.org/10.1016/0022-1694(91)90178-K, 1991.

Gong, L., Widén-Nilsson, E., Halldin, S., and Xu, C. Y.: Large-scale runoff routing with an aggregated network-response


function, J. Hydrol., 368, 237–250, https://doi.org/10.1016/j.jhydrol.2009.02.007, 2009.

Günther, D., Marke, T., Essery, R., and Strasser, U.: Uncertainties in Snowpack Simulations—Assessing the Impact of Model Structure, Parameter Choice, and Forcing Data Error on Point-Scale Energy Balance Snow Model Performance, Water Resour. Res., 55, 2779–2800, https://doi.org/10.1029/2018WR023403, 2019.

Gupta, H. V., Kling, H., Yilmaz, K. K., and Martinez, G. F.: Decomposition of the mean squared error and NSE performance criteria: Implications for improving hydrological modelling, J. Hydrol., 377, 80–91, https://doi.org/10.1016/j.jhydrol.2009.08.003, 2009.

Hanasaki, N., Kanae, S., and Oki, T.: A reservoir operation scheme for global river routing models, J. Hydrol., 327, 22–41, https://doi.org/https://doi.org/10.1016/j.jhydrol.2005.11.011, 2006.

Hersbach, H.: The ERA5 Atmospheric Reanalysis., in: AGU Fall Meeting Abstracts, NG33D-01, 2016.

Huang, M. and Liang, X.: On the assessment of the impact of reducing parameters and identification of parameter uncertainties for a hydrologic model with applications to ungauged basins, J. Hydrol., 320, 37–61, https://doi.org/10.1016/j.jhydrol.2005.07.010, 2006.

Iziomon, M. G., Mayer, H., and Matzarakis, A.: Downward atmospheric longwave irradiance under clear and cloudy skies: Measurement and parameterization, J. Atmos. Solar-Terrestrial Phys., 65, 1107–1116, https://doi.org/https://doi.org/10.1016/j.jastp.2003.07.007, 2003.

Kavetski, D., Fenicia, F., and Clark, M. P.: Impact of temporal data resolution on parameter inference and model identification in conceptual hydrological modeling: Insights from an experimental catchment, Water Resour. Res., 47, W05501, https://doi.org/10.1029/2010WR009525, 2011.

Kazezyılmaz-Alhan, C. M., Medina Jr., M. A., and Richardson, C. J.: A wetland hydrology and water quality model incorporating surface water/groundwater interactions, Water Resour. Res., 43, https://doi.org/https://doi.org/10.1029/2006WR005003, 2007.

Khatami, S., Peel, M. C., Peterson, T. J., and Western, A. W.: Equifinality and Flux Mapping: A New Approach to Model Evaluation and Process Representation Under Uncertainty, Water Resour. Res., 55, 8922–8941, https://doi.org/10.1029/2018WR023750, 2019.

Kling, H., Fuchs, M., and Paulin, M.: Runoff conditions in the upper Danube basin under an ensemble of climate change scenarios, J. Hydrol., 424–425, 264–277, https://doi.org/https://doi.org/10.1016/j.jhydrol.2012.01.011, 2012.

Krause, P., Boyle, D. P., and Bäse, F.: Comparison of different efficiency criteria for hydrological model assessment, Adv. Geosci., 5, 89–97, 2005.

Lehner, B. and Grill, G.: Global river hydrography and network routing: Baseline data and new approaches to study the world's large river systems, Hydrol. Process., 27, 2171–2186, https://doi.org/10.1002/hyp.9740, 2013.

Liang, X., Lettenmaier, D. P., Wood, E. F., and Burges, S. J.: A simple hydrologically based model of land surface water and energy fluxes for general circulation models, J. Geophys. Res., 99, 14,415.14.428, https://doi.org/10.1029/94jd00483, 1994.

Lohmann, D., Nolte-Holube, R., and Raschke, E.: A large scale horizontal routing model to be coupled to land surface


parametrization schemes, Tellus, 48A, 708–721, https://doi.org/10.3402/tellusa.v48i5.12200, 1996.

Lohmann, D., Raschke, E., Nijssen, B., and Lettenmaier, D. P.: Regional scale hydrology: II. Application of the VIC-2L model to the Weser River, Germany, Hydrol. Sci. J., 43, 143–158, https://doi.org/10.1080/02626669809492108, 1998.

Lucas-Picher, P., Arora, V. K., Caya, D., and Laprise, R.: Implementation of a large-scale variable velocity river flow routing algorithm in the Canadian Regional Climate Model (CRCM), Atmos. - Ocean, 41, 139–153, https://doi.org/10.3137/ao.410203, 2003.

Mai, J., R. Craig, J., and A. Tolson, B.: Simultaneously determining global sensitivities of model parameters and model structure, Hydrol. Earth Syst. Sci., 24, 5835–5858, https://doi.org/10.5194/hess-24-5835-2020, 2020.

Mantilla, R.: Physical Basis of Statistical Scaling in Peak Flows and Stream Flow Hydrographs for Topologic and Spatially Embedded Random Self-Similar Channel Networks, University of Colorado, 2007.

McCarthy, G.: The Unit Hydrograph and Flood Routing., in: Unpublished manuscript presented at a conference of the North Atlantic Division, 1938.

Melsen, L., Teuling, A., Torfs, P., Zappa, M., Mizukami, N., Clark, M., and Uijlenhoet, R.: Representation of spatial and temporal variability in large-domain hydrological models: Case study for a mesoscale pre-Alpine basin, Hydrol. Earth Syst. Sci., 20, 2207–2226, https://doi.org/10.5194/hess-20-2207-2016, 2016.

Melsen, L. A., Addor, N., Mizukami, N., Newman, A. J., Torfs, P. J. J. F., Clark, M. P., Uijlenhoet, R., and Teuling, A. J.: Mapping (dis)agreement in hydrologic projections, Hydrol. Earth Syst. Sci., 22, 1775–1791, https://doi.org/10.5194/hess-22-1775-2018, 2018.

Mendoza, P. A., McPhee, J., and Vargas, X.: Uncertainty in flood forecasting: A distributed modeling approach in a sparse data catchment, Water Resour. Res., 48, W09532, https://doi.org/10.1029/2011WR011089, 2012.

Mendoza, P. A., Clark, M. P., Mizukami, N., Gutmann, E. D., Arnold, J. R., Brekke, L. D., and Rajagopalan, B.: How do hydrologic modeling decisions affect the portrayal of climate change impacts?, Hydrol. Process., 30, 1071–1095, https://doi.org/10.1002/hyp.10684, 2016.

Miguez-Macho, G. and Fan, Y.: The role of groundwater in the Amazon water cycle: 1. Influence on seasonal streamflow, flooding and wetlands, J. Geophys. Res. Atmos., 117, 1–30, https://doi.org/10.1029/2012JD017539, 2012.

Mizukami, N., Clark, M. P., Sampson, K., Nijssen, B., Mao, Y., McMillan, H., Viger, R. J., Markstrom, S. L., Hay, L. E., Woods, R., Arnold, J. R., and Brekke, L. D.: mizuRoute version 1: a river network routing tool for a continental domain water resources applications, Geosci. Model Dev., 9, 2223–2238, https://doi.org/10.5194/gmd-9-2223-2016, 2016.

Mizukami, N., Clark, M. P., Gharari, S., Kluzek, E., Pan, M., Lin, P., Beck, H. E., and Yamazaki, D.: A Vector-Based River Routing Model for Earth System Models: Parallelization and Global Applications, J. Adv. Model. Earth Syst., 13, 1–20, https://doi.org/10.1029/2020MS002434, 2021.

Muñoz-Sabater, J., Dutra, E., Agust\'\i-Panareda, A., Albergel, C., Arduini, G., Balsamo, G., Boussetta, S., Choulga, M., Harrigan, S., Hersbach, H., Martens, B., Miralles, D. G., Piles, M., Rodr\'\iguez-Fernández, N. J., Zsoter, E., Buontempo, C., and Thépaut, J.-N.: ERA5-Land: a state-of-the-art global reanalysis dataset for land applications, Earth Syst. Sci. Data, 13,


4349–4383, https://doi.org/10.5194/essd-13-4349-2021, 2021.

Nash, J. and Sutcliffe, J.: River flow forecasting through conceptual models part I - A discussion of principles, J. Hydrol., 10, 282–290, https://doi.org/10.1016/0022-1694(70)90255-6, 1970.

Newman, A. J., Stone, A. G., Saharia, M., Holman, K. D., Addor, N., and Clark, M. P.: Identifying sensitivities in flood frequency analyses using a stochastic hydrologic modeling system, Hydrol. Earth Syst. Sci., 25, 5603–5621, https://doi.org/10.5194/hess-25-5603-2021, 2021.

Niño, Y.: Simple model for downstream variation of median sediment size in Chilean rivers, J. Hydraul. Eng., 128, 934–941, 2002.

Oki, T. and Sud, Y. C.: Design of Total Runoff Integrating Pathways (TRIP)—A Global River Channel Network, Earth Interact., 2, 1–37, https://doi.org/10.1175/1087-3562(1998)002<0001:dotrip>2.3.co;2, 1998.

Olivera, F., Famiglietti, J., and Asante, K.: Global-scale flow routing using a source-to-sink algorithm, Water Resour. Res., 36, 2197–2207, https://doi.org/10.1029/2000WR900113, 2000.

Paiva, R. C. D., Collischonn, W., and Tucci, C. E. M.: Large scale hydrologic and hydrodynamic modeling using limited data and a GIS based approach, J. Hydrol., 406, 170–181, https://doi.org/10.1016/j.jhydrol.2011.06.007, 2011.

Paiva, R. C. D., Buarque, D. C., Collischonn, W., Bonnet, M.-P., Frappart, F., Calmant, S., and Bulhões Mendes, C. A.: Large-scale hydrologic and hydrodynamic modeling of the Amazon River basin, Water Resour. Res., 49, 1226–1243, https://doi.org/10.1002/wrcr.20067, 2013a.

Paiva, R. C. D., Collischonn, W., and Buarque, D. C.: Validation of a full hydrodynamic model for large-scale hydrologic modelling in the Amazon, Hydrol. Process., 27, 333–346, https://doi.org/10.1002/hyp.8425, 2013b.

Poggio, L., de Sousa, L. M., Batjes, N. H., Heuvelink, G. B. M., Kempen, B., Ribeiro, E., and Rossiter, D.: SoilGrids 2.0: producing soil information for the globe with quantified spatial uncertainty, SOIL, 7, 217–240, https://doi.org/10.5194/soil-7-217-2021, 2021.

Price, R. K.: An optimized routing model for flood forecasting, Water Resour. Res., 45, 1–15, https://doi.org/10.1029/2008WR007103, 2009.

Qiu, H., Qi, J., Lee, S., Moglen, G. E. E., McCarty, G. W. W., Chen, M., and Zhang, X.: Effects of temporal resolution of river routing on hydrologic modeling and aquatic ecosystem health assessment with the SWAT model, Environ. Model. Softw., 146, 105232, https://doi.org/10.1016/j.envsoft.2021.105232, 2021.

Salas, F. R. R., Somos-Valenzuela, M. A. A., Dugger, A., Maidment, D. R. R., Gochis, D. J. J., David, C. H. H., Yu, W., Ding, D., Clark, E. P. P., and Noman, N.: Towards Real-Time Continental Scale Streamflow Simulation in Continuous and Discrete Space, J. Am. Water Resour. Assoc., 54, 7–27, https://doi.org/10.1111/1752-1688.12586, 2018.

Sepúlveda, U. M., Mendoza, P. A., Mizukami, N., and Newman, A. J.: Revisiting parameter sensitivities in the variable infiltration capacity model across a hydroclimatic gradient, Hydrol. Earth Syst. Sci., 26, 3419–3445, https://doi.org/10.5194/hess-26-3419-2022, 2022.

Shaad, K.: Evolution of river-routing schemes in macro-scale models and their potential for watershed management, Hydrol.


Sci. J., 63, 1062–1077, https://doi.org/10.1080/02626667.2018.1473871, 2018.

Sheikholeslami, R., Gharari, S., Papalexiou, S. M., and Clark, M. P.: VISCOUS: A Variance-Based Sensitivity Analysis Using Copulas for Efficient Identification of Dominant Hydrological Processes, Water Resour. Res., 1–24, https://doi.org/10.1029/2020wr028435, 2021.

Siqueira, V. A. A., Paiva, R. C. D. C. D., Fleischmann, A. S. S., Fan, F. M. M., Ruhoff, A. L. L., Pontes, P. R. M. R. M., Paris, A., Calmant, S., and Collischonn, W.: Toward continental hydrologic-hydrodynamic modeling in South America, Hydrol. Earth Syst. Sci., 22, 4815–4842, https://doi.org/10.5194/hess-22-4815-2018, 2018.

Sturm, T. W.: Open Channel Hydraulics, Third edit., McGraw-Hill Education, New York, 2021.

Sulla-Menashe, D. and Friedl, M. A.: User Guide to Collection 6 MODIS Land Cover (MCD12Q1 and MCD12C1) Product, https://doi.org/10.5067/MODIS/MCD12Q1, 2018.

Tang, Y., Reed, P., van Werkhoven, K., and Wagener, T.: Advancing the identification and evaluation of distributed rainfall-runoff models using global sensitivity analysis, Water Resour. Res., 43, 1–14, https://doi.org/10.1029/2006WR005813, 2007.

Thober, S., Cuntz, M., Kelbling, M., Kumar, R., Mai, J., and Samaniego, L.: The multiscale routing model mRM v1.0: simple river routing at resolutions from 1 to 50 km, Geosci. Model Dev., 12, 2501–2521, https://doi.org/10.5194/gmd-12-2501-2019, 2019.

Vano, J. A., Das, T., and Lettenmaier, D. P.: Hydrologic Sensitivities of Colorado River Runoff to Changes in Precipitation and Temperature, J. Hydrometeorol., 13, 932–949, https://doi.org/10.1175/JHM-D-11-069.1, 2012.

Verzano, K., Bärlund, I., Flörke, M., Lehner, B., Kynast, E., Voß, F., and Alcamo, J.: Modeling variable river flow velocity on continental scale: Current situation and climate change impacts in Europe, J. Hydrol., 424–425, 238–251, https://doi.org/10.1016/j.jhydrol.2012.01.005, 2012.

Wobus, C., Gutmann, E., Jones, R., Rissing, M., Mizukami, N., Lorie, M., Mahoney, H., Wood, A. W. W., Mills, D., and Martinich, J.: Climate change impacts on flood risk and asset damages within mapped 100-year floodplains of the contiguous United States, Nat. Hazards Earth Syst. Sci., 17, 2199–2211, https://doi.org/10.5194/nhess-17-2199-2017, 2017.

Wood, E. F., Lettenmaier, D. P., and Zartarian, V. G.: A land-surface hydrology parameterization with subgrid variability for general circulation models, J. Geophys. Res. Atmos., 97, 2717–2728, https://doi.org/https://doi.org/10.1029/91JD01786, 1992.

Yamazaki, D., Kanae, S., Kim, H., and Oki, T.: A physically based description of floodplain inundation dynamics in a global river routing model, Water Resour. Res., 47, 1–21, https://doi.org/10.1029/2010WR009726, 2011.

Yamazaki, D., De Almeida, G. A. M., and Bates, P. D.: Improving computational efficiency in global river models by implementing the local inertial flow equation and a vector-based river network map, Water Resour. Res., 49, 7221–7235, https://doi.org/10.1002/wrcr.20552, 2013.

Ye, A., Duan, Q., Zhan, C., Liu, Z., and Mao, Y.: Improving kinematic wave routing scheme in Community Land Model, Hydrol. Res., 44, 886–903, https://doi.org/10.2166/nh.2012.145, 2013.

Zhao, F., Veldkamp, T. I. E., Frieler, K., Schewe, J., Ostberg, S., Willner, S., Schauberger, B., Gosling, S. N., Schmied, H. M., Portmann, F. T., Leng, G., Huang, M., Liu, X., Tang, Q., Hanasaki, N., Biemans, H., Gerten, D., Satoh, Y., Pokhrel, Y.,

https://doi.org/10.5194/hess-2022-338
Preprint. Discussion started: 7 October 2022


Hydrology and Earth System Sciences
Discussions

630 Stacke, T., Ciais, P., Chang, J., Ducharne, A., Guimberteau, M., Wada, Y., Kim, H., and Yamazaki, D.: The critical role of the routing scheme in simulating peak river discharge in global hydrological models, Environ. Res. Lett., 12, https://doi.org/10.1088/1748-9326/aa7250, 2017.

ZHAO, R.-J.: The Xinanjiang model, Proc. Oxford Symp., 1980.

635

https://doi.org/10.5194/hess-2022-338
Preprint. Discussion started: 7 October 2022


Hydrology and Earth System Sciences
Discussions

**Table 1. Stream Gauge Stations in the Cautín at Cajón River basin. Annual streamflow at each station was obtained from daily records for the period April 1985-March 2020.**

| | Station Name | Abbreviation | Latitude (°S) | Longitude (°W) | Area ($km^2$) | Elevation (m a.s.l.) | Mean Annual Flow ($m^3/s$) |
|---|---|---|---|---|---|---|---|
| 1 | Collín at Codahue | CatCd | 38.58 | 72.19 | 259 | 250 | 12 |
| 2 | Muco at Muco Bridge | MatPM | 38.61 | 72.39 | 651 | 250 | 24 |
| 3 | Cautín at Rariruca | CatRR | 38.43 | 72.01 | 1305 | 425 | 86 |
| 4 | Cautín at Cajón | CatC | 38.69 | 72.50 | 2770 | 130 | 130 |

**Table 2. VIC model parameters sampled in this study.**

| Parameter | Units | Lower value | Upper value | Description |
|---|---|---|---|---|
| Infilt | - | 0.01 | 0.99 | Variable infiltration curve parameter |
| $D_s$ | - | 0.1 | 0.9 | Fraction of $D_{s_{max}}$ where non-linear baseflow occurs |
| $D_{s_{max}}$ | mm/d | 0.1 | 300 | Maximum velocity of baseflow |
| $W_s$ | - | 0.1 | 0.9 | Fraction of maximum soil moisture where non-linear baseflow occurs |
| expt | - | 3.1 | 10 | Exponent of Campbell's equation for hydraulic conductivity |
| $d_{max}$<br>$d_1$<br>$d_2$<br>$d_3$ | m | 0.5<br>0.05 $d_{max}$<br>0.21 $d_{max}$<br>0.74 $d_{max}$ | 5<br>0.2 $d_{max}$<br>0.7 $d_{max}$<br>0.1 $d_{max}$ | Depth of soil layers 1, 2 and 3 |
| $K_{sat}$ | mm/d | 1 | 1000 | Saturated hydraulic conductivity |
| $T_{max,snow}$ | (°C) | -10 | 10 | Maximum temperature for snowfall |
| $\alpha_{thaw}$ | - | 0.75 | 0.90 | Decay of albedo |
| $\alpha_{new}$ | - | 0.85 | 0.95 | Maximum albedo for fresh snow |

640

https://doi.org/10.5194/hess-2022-338
Preprint. Discussion started: 7 October 2022




Hydrology and Earth System Sciences
Discussions

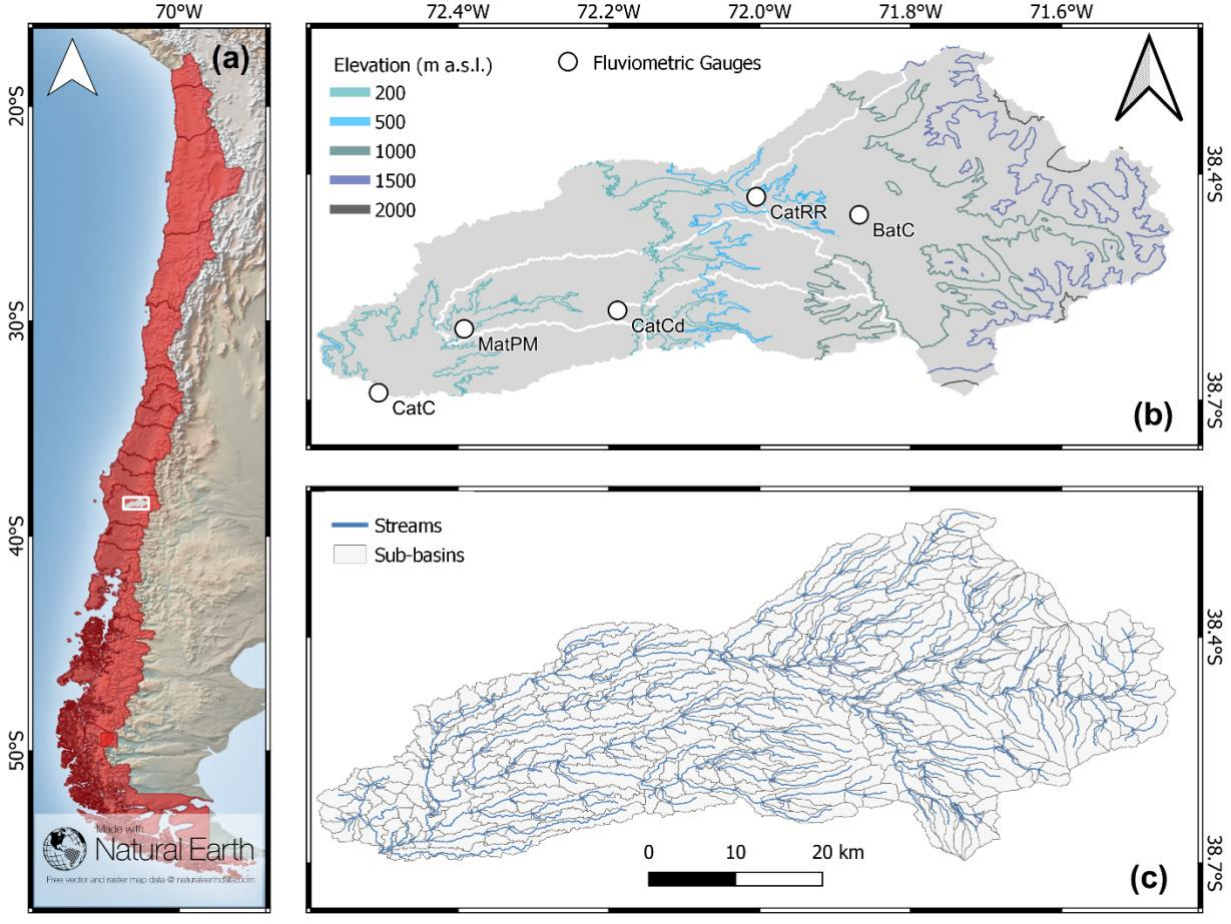


**Figure 1. (a) Location of the Cautín at Cajón River basin in Chile (CatC, 2770 km$^2$). (b) location of outlet and inner stream gauge stations (white circles) and contributing drainage areas (white lines). The inner stations are Muco at Muco bridge (MatPM, 651 km$^2$), Collín at Codahue (CatCD, 259 km$^2$) and Cautín at Rariruca (CatRR, 1305 km$^2$). (c) Digital river network and sub-basin boundaries used in mizuRoute.**

https://doi.org/10.5194/hess-2022-338
Preprint. Discussion started: 7 October 2022


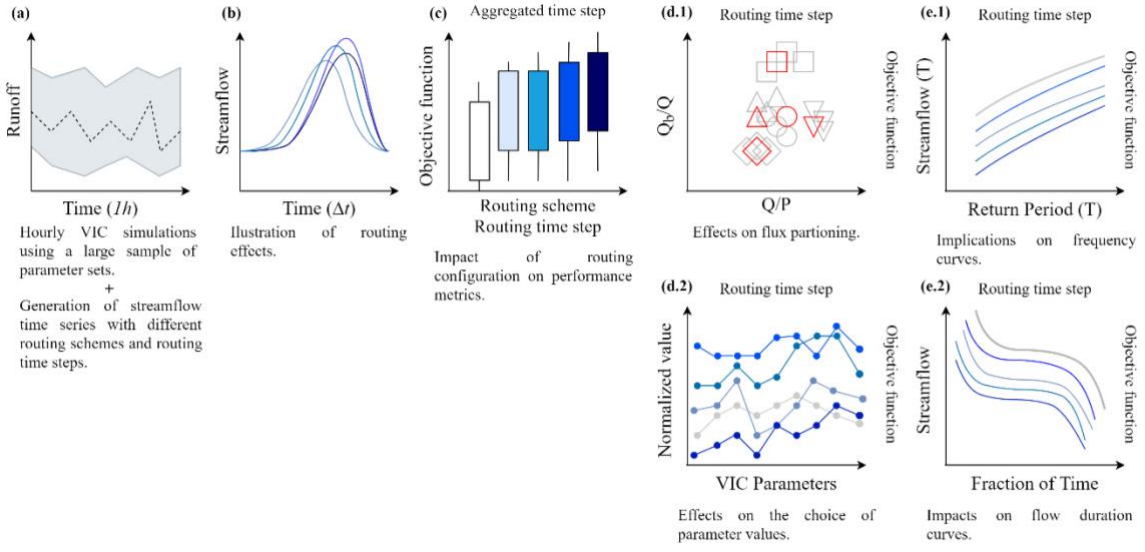


**Figure 2. Overview of the analysis framework used here. (a) VIC model simulations are conducted at hourly time steps for 3500 parameter sets. (b) Each runoff time series is aggregated to four additional time steps (3, 6, 12, 24 h), and the new time series are routed with four schemes (IRF, KWT, MC, DW) to produce 3500 (VIC parameters) x 5 (time steps) x 5 (Inst + four routing schemes) modeling configurations. (c) For each configuration, we compute performance metrics (KGE, NSE, NSE-log; see section 3.4). (d) We analyse simulated mean annual water balance and baseflow contribution to total runoff, and compare the best parameters sets for each configuration in terms of their normalized values. (e) Finally, we analyse the implications of routing configurations on flood frequency and flow durations curves.**

https://doi.org/10.5194/hess-2022-338
Preprint. Discussion started: 7 October 2022


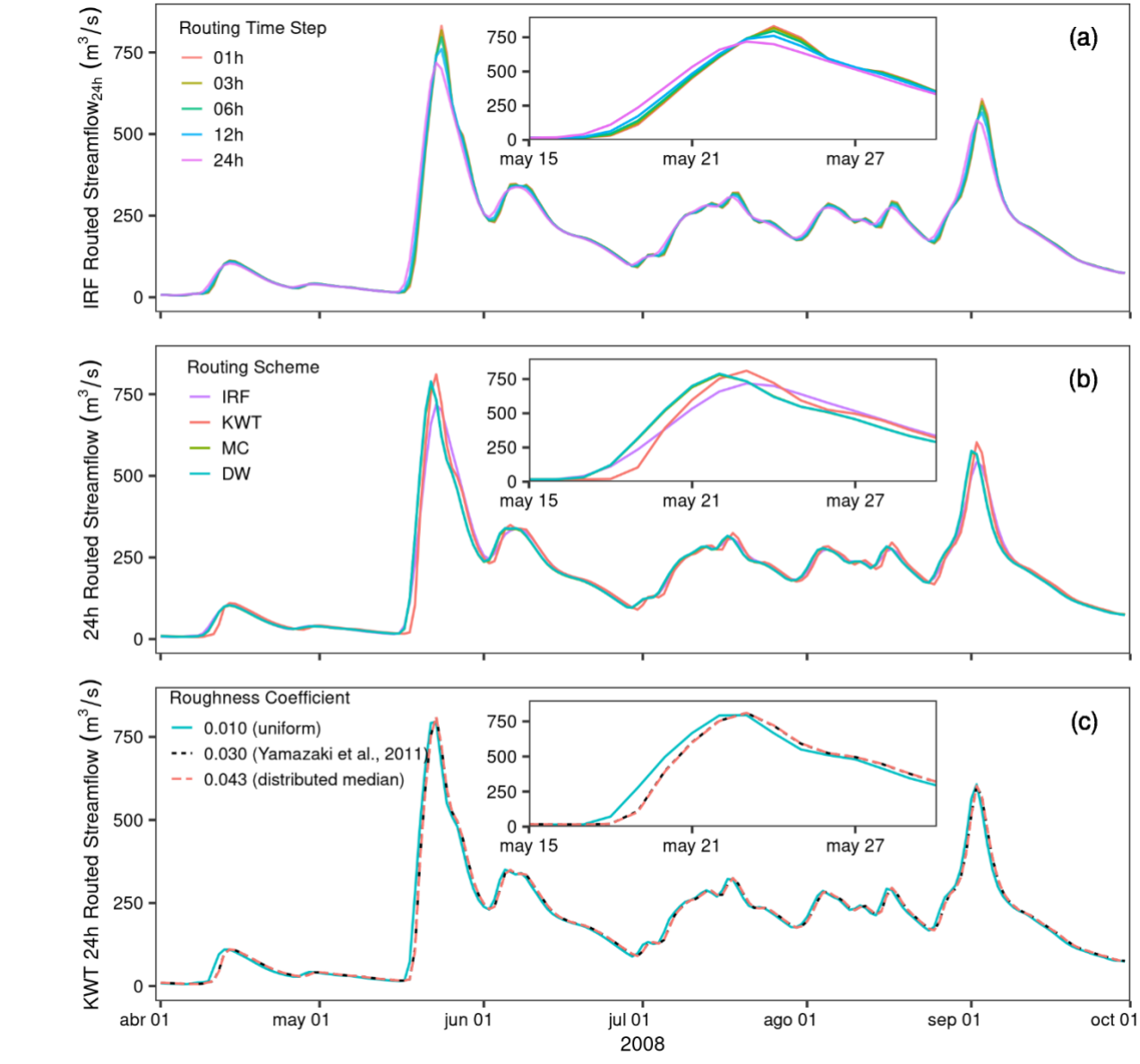


**Figure 3. Time series with simulated daily streamflow at Cautín at Cajón, obtained from hourly VIC runoff outputs routed with different configurations of mizuRoute: (a) application of IRF with five different routing time steps; (b) effects of different routing schemes on daily routed streamflow; and (c) effects of the spatial distribution considered for the Manning's roughness coefficient ($n$) on daily streamflow simulations when applying the kinematic wave routing scheme (KWT) (see text for details).**

https://doi.org/10.5194/hess-2022-338
Preprint. Discussion started: 7 October 2022


Hydrology and Earth System Sciences
Discussions

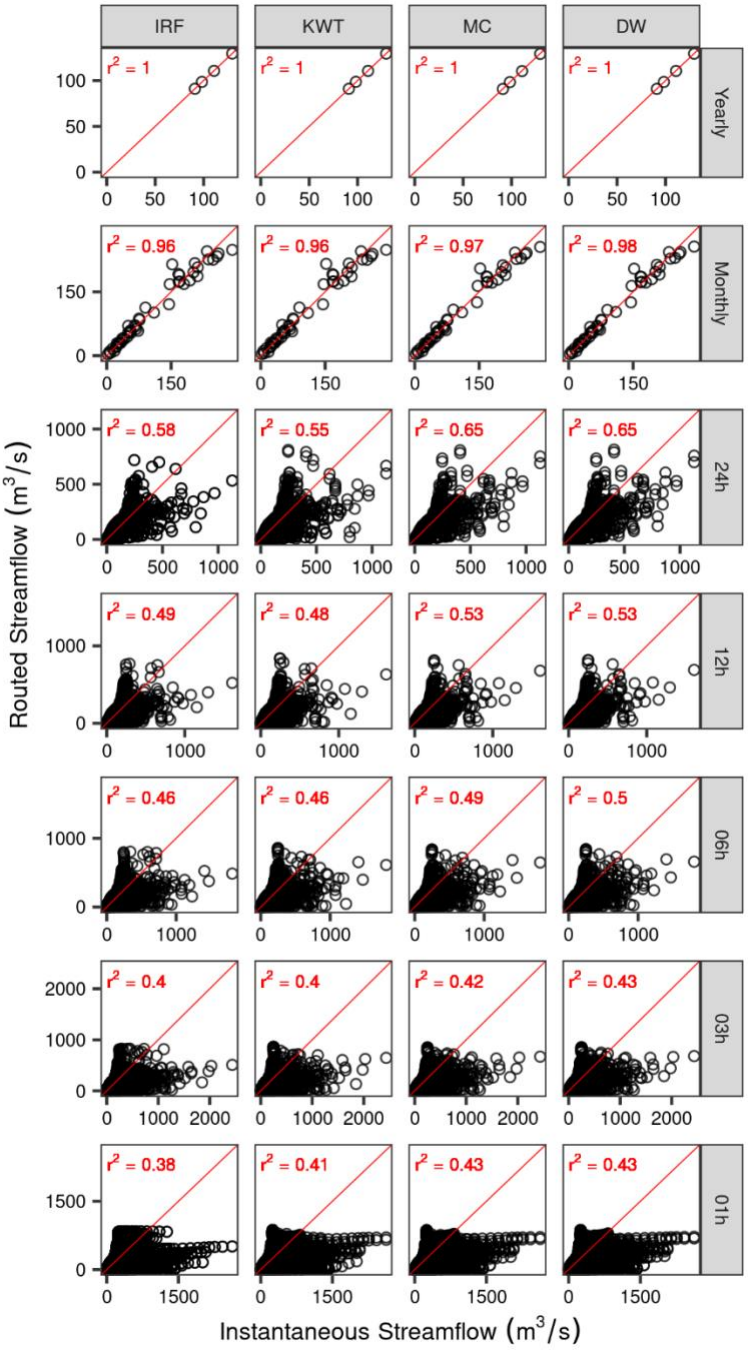


**Figure 4. Simulated streamflow (VIC+mizuRoute) vs. instantaneous VIC runoff for the period April/2008-March/2012, using different time steps (rows) and routing schemes (columns): instantaneous runoff (Inst), Impulse Response Function (IRF), Kinematic Wave Tracking (KWT), Muskingum-Cunge (MC) and Diffusive Wave (DW). Mean yearly**

https://doi.org/10.5194/hess-2022-338
Preprint. Discussion started: 7 October 2022


Hydrology and Earth System Sciences
Discussions

**and monthly streamflow are computed from daily values. The 1:1 line is displayed in red with the coefficient of determination ($R^2$).**

https://doi.org/10.5194/hess-2022-338
Preprint. Discussion started: 7 October 2022



**Figure 5. Impact of routing scheme and routing time step on performance metrics (rows) computed for the period April/2008-March/2012, using different discharge temporal resolutions (columns) across a large sample of VIC parameter sets obtained through Latin Hypercube Sampling (see text for details). The results are presented for instantaneous runoff (Inst), Impulse Response Function (IRF), Kinematic Wave Tracking (KWT), Muskingum-Cunge (MC) and Diffusive Wave (DW).**

https://doi.org/10.5194/hess-2022-338
Preprint. Discussion started: 7 October 2022


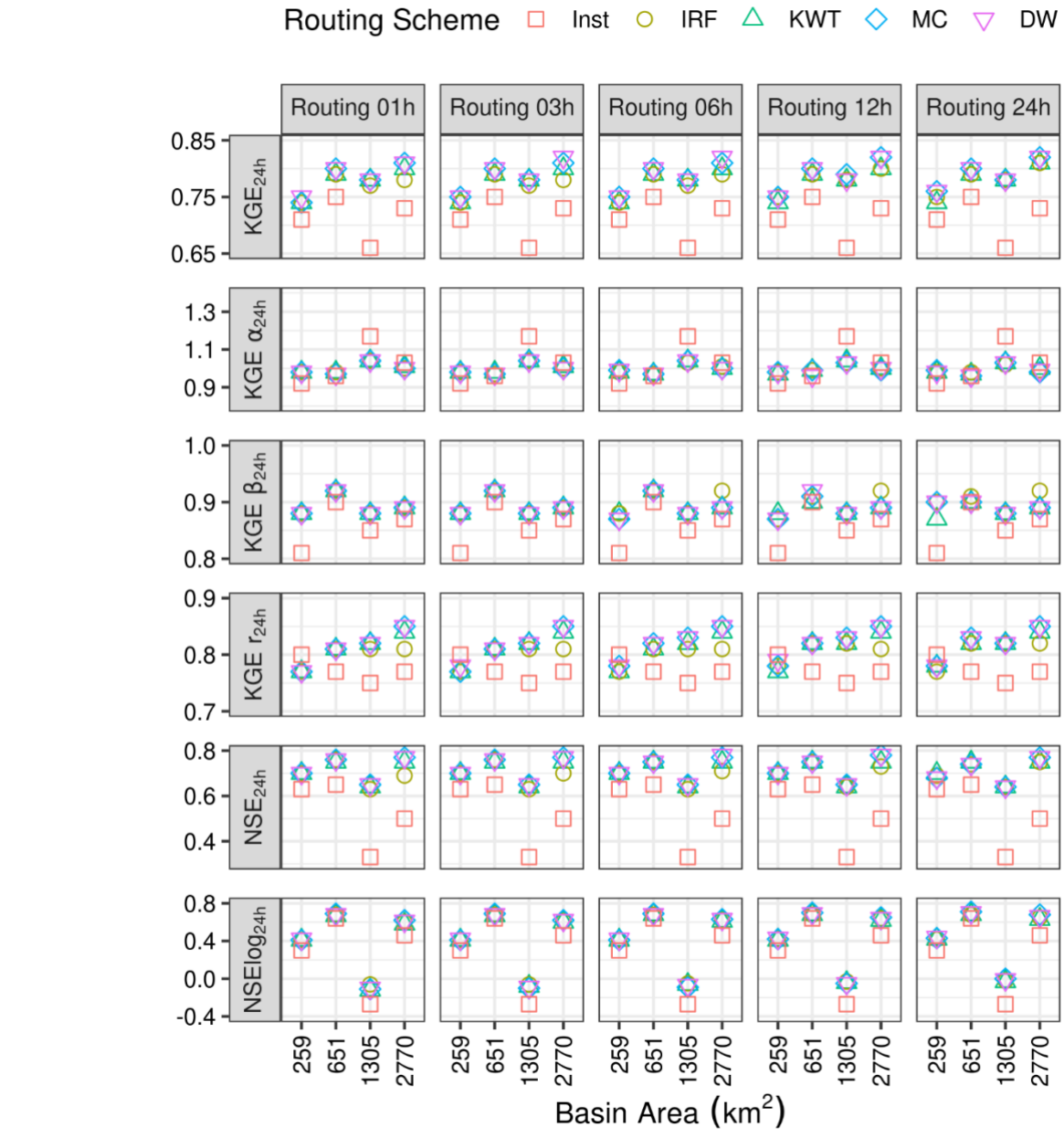


675

**Figure 6. Best performance metric obtained with daily flows for a given objective function (rows), routing time step (columns) and routing scheme for the period April/2008-March/2012. For completeness, the KGE components associated to the best KGE value are included. The results are presented for instantaneous runoff (Inst), Impulse Response Function (IRF), Kinematic Wave Tracking (KWT), Muskingum-Cunge (MC) and Diffusive Wave (DW).**

https://doi.org/10.5194/hess-2022-338
Preprint. Discussion started: 7 October 2022


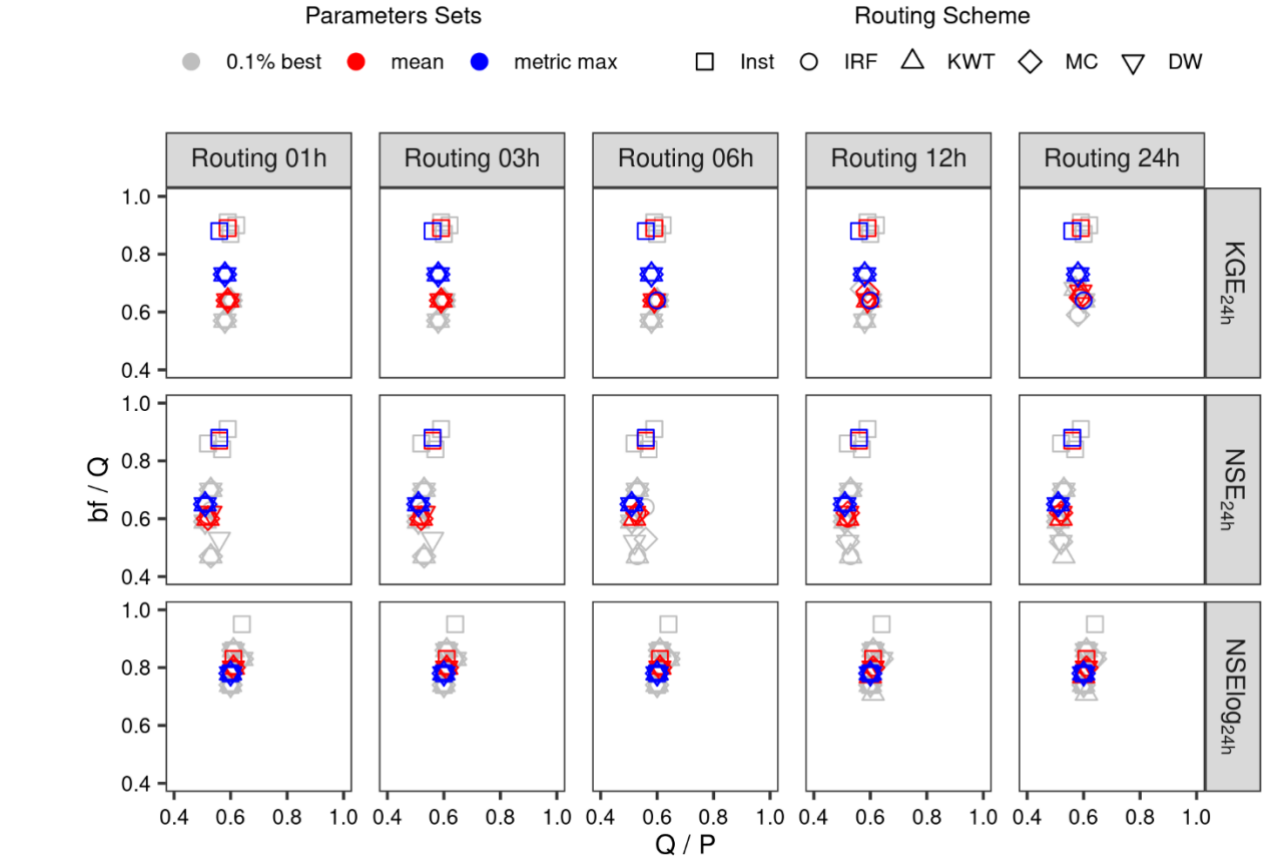


**Figure 7. Effects of objective function (rows), routing time step (columns) and routing scheme on simulated mean annual water balance (characterized with the annual runoff ratio, x-axis) and the baseflow ratio (y-axis) obtained for the 0.1% best VIC parameter sets (period April/2008-March/2012). The results are presented for instantaneous runoff (Inst), Impulse Response Function (IRF), Kinematic Wave Tracking (KWT), Muskingum-Cunge (MC) and Diffusive Wave (DW). In each panel, the results obtained with the parameter set (among the 3500 samples) that maximizes each metric are displayed in blue; results from a small ensemble (n = 4) with the best 0.1% VIC parameter sets are displayed in grey, and the average partitioning obtained from that ensemble is shown in red.**

https://doi.org/10.5194/hess-2022-338
Preprint. Discussion started: 7 October 2022


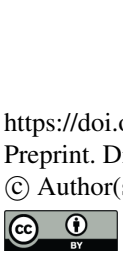

Hydrology and Earth System Sciences
Discussions

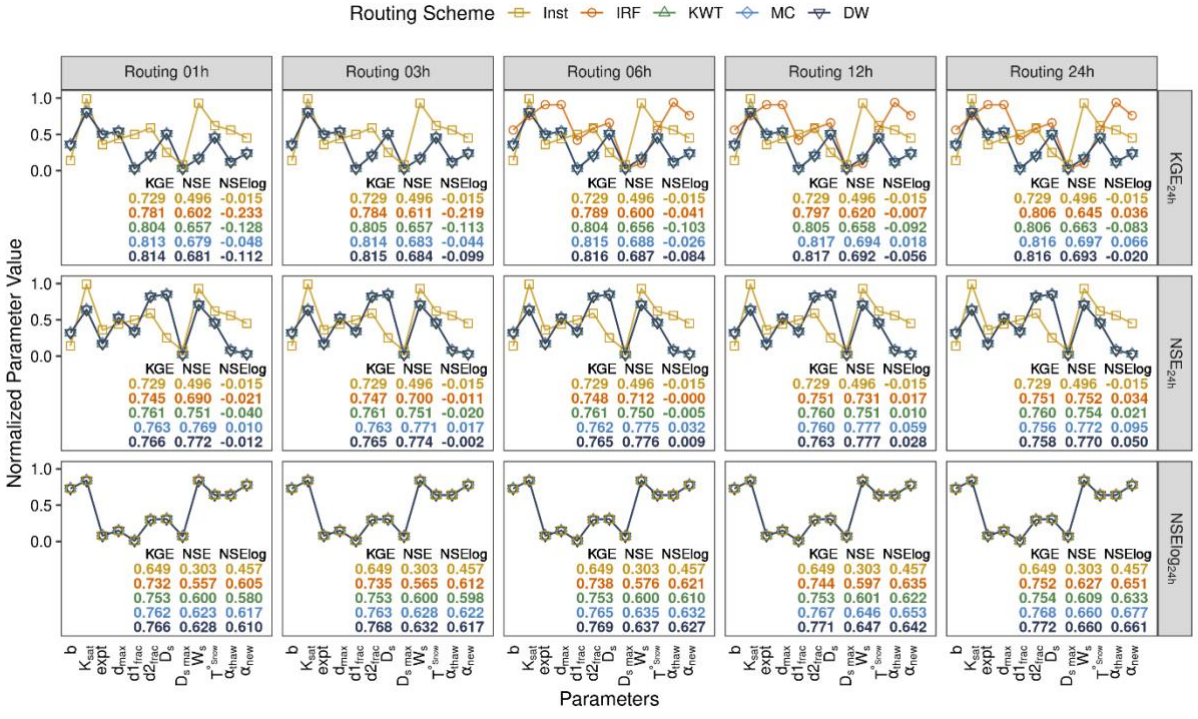


**Figure 8. Normalized VIC parameter values associated to the best performance metric (period April/2008 – March/2012) obtained from the 3500 parameter sets produced with LHS, given a combination of routing scheme and routing time step. The coloured numbers indicate the best objective function value and associated values for the other two metrics. The results are presented for daily instantaneous runoff (Inst), Impulse Response Function (IRF), Kinematic Wave Tracking (KWT), Muskingum-Cunge (MC) and Diffusive Wave (DW).**

https://doi.org/10.5194/hess-2022-338
Preprint. Discussion started: 7 October 2022


Hydrology and Earth System Sciences
Discussions

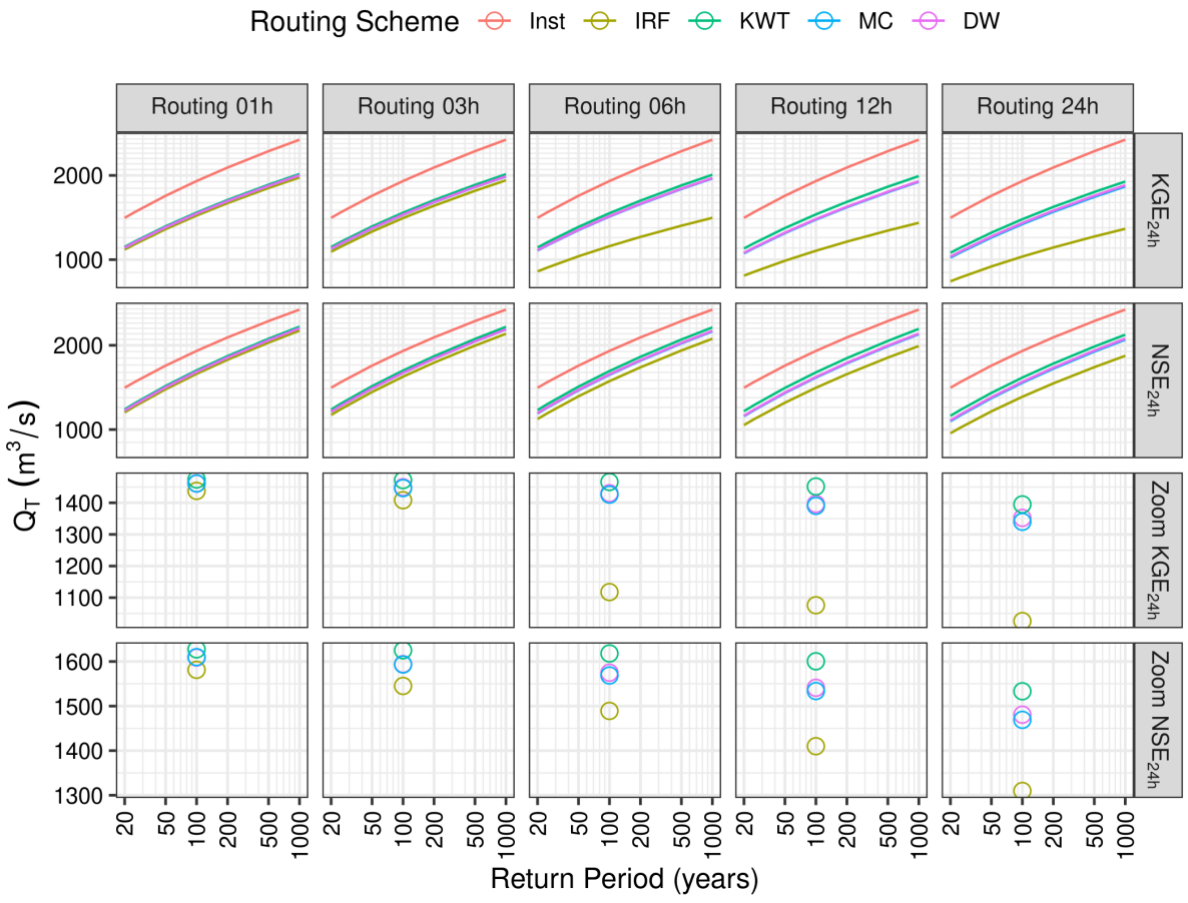


695 **Figure 9. Frequency curves for annual maximum daily flows (y-axis) derived from numerical simulations conducted with different routing schemes, routing time steps (columns) and calibration objective function (rows). All frequency curves are computed from annual time series of n = 35 annual maximum daily flows (April/1985 – March/2020) using a Log-Normal density function. The results are presented for instantaneous runoff (Inst), Impulse Response Function (IRF), Kinematic Wave Tracking (KWT), Muskingum-Cunge (MC) and Diffusive Wave (DW).**

https://doi.org/10.5194/hess-2022-338
Preprint. Discussion started: 7 October 2022


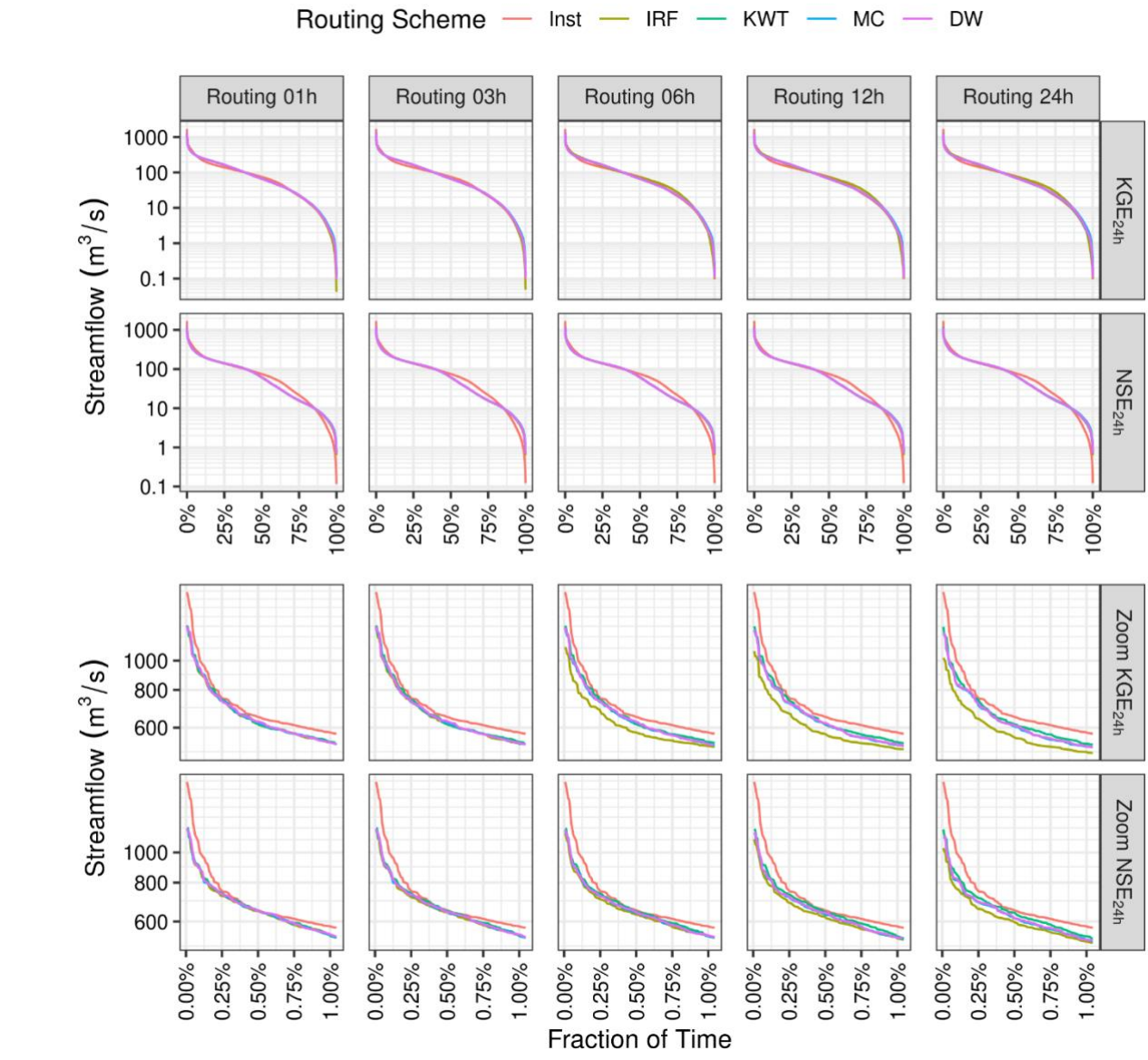


700

**Figure 10. Mean daily flow duration curves for the period April/1985 – March/2020 derived from different routing schemes, routing time steps (columns) and calibration objective function (rows). The results are presented for daily instantaneous runoff (Inst), Impulse Response Function (IRF), Kinematic Wave Tracking (KWT), Muskingum-Cunge (MC) and Diffusive Wave (DW) routing schemes.**